Available online at www.sciencedirect.com
SCIENCE DIRECT
Journal of Molecular Catalysis A: Chemical 246 (2006) 128–135
JOURNAL OF MOLECULAR CATALYSIS A: CHEMICAL
www.elsevier.com/locate/molcata

Catalytic and redox properties of nano-sized $La_{0.8}Sr_{0.2}Mn_{1-x}Fe_xO_{3-\delta}$ mixed oxides synthesized by different routes

M.R. Pai [a], B.N. Wani [a], B. Sreedhar [c], S. Singh [b], N.M Gupta [a,*]

[a] *Chemistry Division, Bhabha Atomic Research Centre, Trombay, Mumbai 400 085, India*
[b] *Solid State Physics Division, Bhabha Atomic Research Centre, Trombay, Mumbai 400 085, India*
[c] *Inorganic and Physical Chemistry Division, Indian Institute of Chemical Technology, Hyderabad 500 007, India*

Received 1 June 2005; received in revised form 13 October 2005; accepted 13 October 2005
Available online 28 November 2005

Abstract

The $La_{0.8}Sr_{0.2}Mn_{1-x}Fe_xO_{3-\delta}$ (LSMF) samples of perovskite-type structure, with the value of x ranging from 0 to 1.0 were synthesized by using two different methods, viz. nitrate and solid-state routes, and by calcining at different temperatures. Efforts were directed to identify the microstructural and morphological properties responsible to the substitution-induced modification in catalytic behavior of these materials. The XRD studies showed that the incorporation of iron resulted in single-phase samples of orthorhombic symmetry instead of the rhombohedral symmetry of the parent LSM perovskite. The Mössbauer spectra revealed that iron existed in trivalent state but in three distinctive coordinative environments. At one of these sites, iron was found to be paramagnetic in nature and the concentration of these species decreased with the increasing iron content. On the other hand, XPS results revealed that the valence state of 'B' site cations, Fe and Mn, was different at the surfaces of the sample as compared to the bulk. No significant segregation of an individual metal was noticed at the surface layer. At the same time, the particles of Fe-containing samples were smaller in size as compared to LSM and it was found to have a direct impact on the lowered reduction temperature and the enhanced catalytic activity of LSMF samples. The results of our study reveal that in addition to the oxygen ion vacancies generated in the lattice due to multiple oxidation states of 'B' site cations, the symmetry around a substituent cation and the subtle changes in particle morphology may also play an important role in deciding the catalytic behavior of the LSMF perovskites.

Keywords: La–Sr–Mn–Fe–O perovskites; Catalytic properties; Redox properties; Role of particle morphology; Role of oxygen ion vacancies

1. Introduction

Perovskite-type mixed oxides (ABO_3) have been the subject of extensive studies during past few decades, because these materials offer large scope for tailoring of their structure by making cationic substitutions at A or B sites. These structural changes are in turn known to influence their catalytic, electronic and magnetic properties to a considerable extent [1–10]. For applications in catalysis, in particular, the lanthanide perovskites (A = La, B = first-row transition metal) have received the most attention, because of their thermodynamic stability at reasonably high temperatures and at the same time high catalytic activity for oxidation reactions concerning pollution abatement. Substitutions at both the A and B site of these lanthanides are found to modify the catalytic properties in different ways. Thus, the substitution of La by Ca, Sr or Ba is known to improve oxygen ion mobility and, hence, the reducibility of the cation at B site. Similarly, the multiple substitutions at catalytically active 'B' sites by some aliovalent transition metal cations lead to enhanced catalytic activity due to synergistic valence changes and resultant non-stoichiometry-related micro-structural defects introduced into the lattice. As has been demonstrated in recent researches carried out in our laboratories, the substitution-induced enhancement in catalytic activity has been observed in the mixed-metal oxides of other structures, e.g. pyrochlores and scheelites, as well [11–17]. Overall, such effects have been attributed to various factors, such as: structural rearrangement arising due to change in oxygen content, increase in lattice vacancies leading to higher oxide ion mobility, synergistic role of mixed valence states of cations at 'B' site and the segregation of active metal components at the surface layer. These aspects

* Corresponding author at: Emeritus Scientist (CSIR), National Chemical Laboratory, Pune 411008, India.
E-mail address: nm.gupta@ncl.res.in (N.M Gupta).

1381-1169/$ – see front matter © 2005 Elsevier B.V. All rights reserved.
doi:10.1016/j.molcata.2005.10.016

have been investigated for a large number of mixed metal oxide compositions, and the subject has been reviewed in various articles [18–20]. Nevertheless, no concerted efforts have been made as yet to explore how morphological changes resulting from cationic substitution, i.e. changes in the size, shape and surface area of the sample particles, may contribute to the catalytic behavior of the perovskites.

The double perovskites of composition $La_{0.8}Sr_{0.2}MnO_{3-\delta}$ (LSM) are important, not only as cathode material for solid oxide fuel cells but also as prospective oxidation catalysts. In this paper, we report on the surface composition, structural characteristics, redox properties and catalytic activity of LSM oxides as a function of Fe substitution. Our goal was to examine how different microstructural and morphological changes, resulting from the different procedures adopted for synthesis of these samples, may influence the catalytic properties of these oxides. For this purpose, a series of mixed oxides of composition $La_{0.8}Sr_{0.2}Mn_{1-x}Fe_xO_{3-\delta}$ ($x = 0$–1.0) were synthesized by two alternative procedures, i.e. solid-state route and solution route, and were subjected to calcination at different temperatures. The samples were characterized systematically, in order to differentiate between the relevant physical and chemical properties of differently synthesized samples. The phase characteristics, crystallite size and surface area of the samples were examined by using powder X-ray diffraction (XRD) and N_2 adsorption techniques. The techniques of X-ray photoelectron and Mössbauer spectroscopies were employed to identify the oxidation state of the constituents, at the surface and in the bulk of these multi-metal oxides. The reduction/oxidation (redox) behavior of these samples was studied by recording the temperature-programmed reduction (TPR) profiles. The catalytic behavior of these materials was evaluated for CO oxidation as a model reaction.

2. Experimental

One molar nitrate solutions of component cations were mixed together in appropriate proportion, so as to achieve a desired composition of $La_{0.8}Sr_{0.2}Mn_{1-x}Fe_xO_{3-\delta}$ (abbreviated as LSMF) samples while preparing through solution route. After drying at 80 °C, the resultant solidus pulp was calcined at 550 °C and, then, at 900 °C for 24 h duration, and the completion of the reaction was ascertained from powder XRD analysis. In the exceptional case of a Fe-free sample (i.e. LSM), the completion of the reaction was attained only at the temperature of 1100 °C or above. Some representative samples were prepared by solid-state route also. For this, the oxides of the constituent metals were ground thoroughly, were palletized and, then, calcined in three stages, i.e. at 900, 1100 and 1400 °C. The samples were ground well and palletized after each of these calcinations steps, in order to achieve completion of the reaction. Some of the representative samples prepared by solution route were also calcined at an elevated temperature of 1400 °C so as to make a comparative evaluation. The average particle size of different samples was obtained using Scherrer equation. A Quantachrome Autosorb-1 analyzer was employed for measurement of surface area by recording the nitrogen adsorption isotherms. Powder XRD patterns were recorded on a Philips X-ray diffractometer (PW 1710, Ni -filtered Cu Kα radiation), using silicon as an external standard. These patterns were indexed to generate their lattice dimensions using a powder program.

^{57}Fe Mössbauer spectra of substituted samples were obtained at ambient temperature (298 K) in a constant acceleration mode using a ^{57}Co source in Rh matrix (50 mCi). The samples were mixed with a diluting agent, i.e. Li_2CO_3, and the iron content was maintained constant at 0.2 mg cm^{-2} in all the absorbers. The experimental data were fitted with the help of a least square curve-fitting program and the isomer shift values are reported with respect to α-Fe as standard.

The XPS spectra were recorded on a KRATOS AXIS 165 spectrometer equipped with a dual anode (Mg and Al) system, using the Mg Kα anode (1253.6 eV) source. The pressure in the spectrometer was ∼10^{-9} Torr. Carbon 1s photoelectron line (284.6 eV) was used for energy calibration. Spectra were deconvulated with the help of Sun Solaris based Vision-2 curve resolver. The binding energies obtained for identical samples were in general reproducible to within ±0.1 eV.

For evaluating the reduction behavior as a function of sample composition, temperature-programmed reduction (TPR) profiles were recorded on a TPDRO-1100 analyzer (Thermoquest, Italy), equipped with a thermal conductivity detector. H_2 (5%) + Ar gas mixture was employed for recording of the reduction profiles. All the samples were pretreated in an inert atmosphere at 350 °C for 2 h prior to recording of the first TPR run. A soda-lime trap was connected in line so as to remove any moisture released during the TPR runs. The data were plotted in temperature range 25–900 °C, at a heating rate of 6 °C min^{-1}.

A fixed-bed continuous-flow tubular reactor made of quartz was employed for the measurement of catalytic activity of different samples for CO oxidation reaction. For each experiment, 0.1 g of a sample was placed between two quartz wool plugs (bed lengih ∼1 mm), the reactant (CO:O_2:He = 2:1:17) flow being at 15 ml min^{-1}. Effluents were sampled and analyzed on a gas chromatograph (Porapak-Q column and thermal conductivity detector).

3. Results

Table 1 gives representative particle size data on $La_{0.8}Sr_{0.2}Mn_{1-x}Fe_x0_{3-\delta}$ ($x = 0$–l.0) samples synthesized by using above-mentioned two routes. As seen in these data, the particle size of 15–18 nm for iron-containing samples was almost half as compared to the samples of extreme composition (∼30 nm), the preparation and calcination conditions being identical. Also, the crystallite size was large (48–50 nm) for the samples prepared by solid-state route and calcined at 1400 °C. This particle size trend was reflected in the surface area of the substituted samples as well. Thus, the substituted samples prepared via nitrate route exhibited a surface area in range 5–7 m^2 g^{-1} the value changing only marginally with Fe content. The corresponding surface area for unsubstituted samples with the x value of 0 and 1 was in the range of 3.4–3.8 m^2 g^{-1}.

Table 1
Particle size (nm) of LSMF samples prepared through different routes

Sample	Label	Nitrate route (calcination 900 °C)	Solid-state route (calcination 1400 °C)
$La_{0.8}Sr_{0.2}MnO_3$	LSM	27	50
$La_{0.8}Sr_{0.2}Mn_{0.8}Fe_{0.2}O_3$	LSMF2	16	48
$La_{0.8}Sr_{0.2}Mn_{0.6}Fe_{0.4}O_3$	LSMF4	16	–
$La_{0.8}Sr_{0.2}Mn_{0.4}Fe_{0.6}O_3$	LSMF6	15	49
$La_{0.8}Sr_{0.2}Mn_{0.2}Fe_{0.8}O_3$	LSMF8	24	–
$La_{0.8}Sr_{0.2}FeO_3$	LSF	29	–

3.1. XRD

The XRD patterns of LSMF samples, synthesized through solution route and calcined at 900 °C, are shown in Fig. 1 as a function of Fe-content. In general, the iron substitution helped in the synthesis of single-phase materials at a relatively lower temperature, as compared to corresponding Fe-free LSM sample. Thus, the reflections marked with # in Fig. 1a for a LSM sample ($x = 0$, calcined at 900 °C) match with the powder XRD pattern of rhombohedral $La_{0.9}Sr_{0.1}MnO_{3.15}$ (PC-PDF no. 47-0444). At the same time, we observe certain weak reflections (marked *) in this figure due to un-reacted La_2O_3. The completion of the reaction was observed on calcination of the sample at 1100 °C and the relevant XRD pattern is shown in Fig. 1b. In the case of all iron-substituted samples, the reaction was found to be complete at 900 °C (Fig. 1c–f) and all the synthesized samples exhibited an orthorhombic symmetry irrespective of the iron content. However, a change of symmetry to rhombohedral was observed when the LSMF samples were calcined at 1100 °C, as shown in Fig. 1g for a representative sample LSMF2. Corresponding lattice parameters are also included in Table 2. The data given in Tables 1 and 2 show that the change of symmetry to orthorhombic in case of the low-temperature synthesized LSMF samples is accompanied with a considerable decrease in the cell volume and also in the decrease of the crystallite size from ~27 to 15 nm. Our results, thus, show that Fe-doping helped in stabilization of orthorhombic phase of LSM even at low synthesis temperatures (i.e. ~900 °C). This is in contrast to a similar study reported earlier, where the orthorhombic phase of lanthanum–strontium ferromanganites, i.e $(La_{1-x}Sr_x)(Mn_{1-y}Fe_y)O_{3\pm\delta}$ samples with x and $y = 0.2$, 0.5 and 0.7, was found to be stabilized only at ~1300 °C [21].

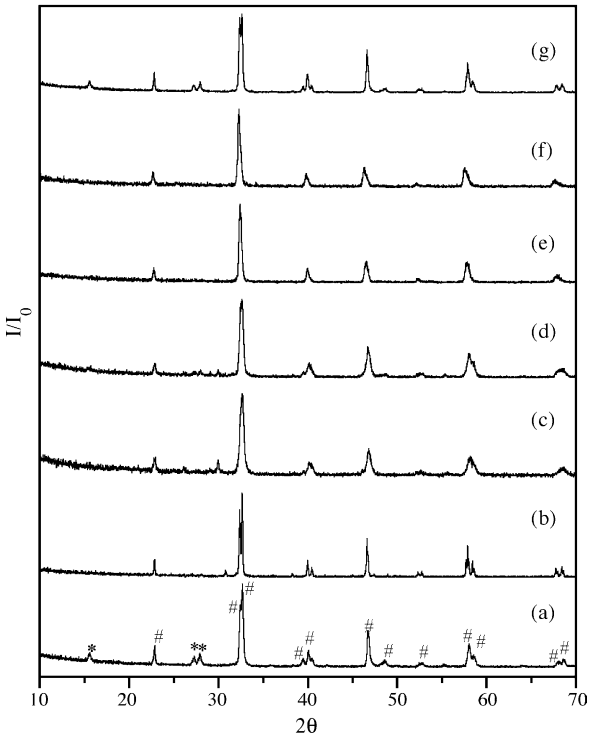

Fig. 1. XRD patterns of $La_{0.8}Sr_{0.2}Mn_{1-x}Fe_xO_{3-\delta}$ (LSMF) samples as a function of Fe-content and calcination temperature. Curves (a) LSM, (b) LSM (1100 °C), (c) LSMF2, (d) LSMF6, (e) LSMF8, (f) LSF and (g) LSMF2 (1100 °C). Calcination temperature for curves a and c–f, is 900 °C.

3.2. XPS

The core-level XPS spectra corresponding to La 3d and Sr 3d lines were unaffected of Fe substitution and were basically similar to those reported for LSM samples by other authors [22,23]. Thus, the main La $3d_{5/2}$ and $3d_{3/2}$ lines were observed at binding energy (BE) values of 834.59 and 851.55 eV, with a separation of approximately 16.96 eV. These La 3d lines were accompanied with equally intense satellite lines appearing at 838.12 and 855.06 eV, arising due to electron transfer from oxygen ligands to the La 4f orbital [22]. Sputtering (Ar^+, 5 keV) of the sample for varying periods of time gave similar spectrum besides a shift in binding energy to a lower value by 0.9 ± 0.1 eV. This BE shift was seen more clearly in case of the iron-substituted samples.

Interesting results were obtained in case of the Fe (2p) and Mn (2p) core level XPS signals. In both these cases overlapping bands were observed signifying the presence of multiple oxidation states of these elements, the relative concentration of which changed as a result of sputtering and also as a function of iron content. The Mn 2p and Fe 2p XPS spectra are shown in Figs. 2 and 3, respectively, for a representative LSMF2 sample. The resolution of these spectra into component peaks is shown by the dotted curves in these figures. In the case of Mn XPS spectrum, we observe two lines at 642.6 and 641.4 eV (Fig. 2). The position of these signals remained unchanged within ±0.1 eV in the case of the substituted samples. Both these Mn $2p_{3/2}$ signals exhibited a negative shift in BE, to the extent of 0.6–0.8 eV, when the sample were sputtered with Ar^+ for 10–30 min. A similar shift was observed in case of Fe 2p XPS signals, as shown in Fig. 3.

Table 2
Effect of calcination temperature on cell parameters of $La_{0.8}Sr_{0.2}Mn_{1-x}Fe_xO_{3-\delta}$ samples

Calcination temperature (°C)	Value of x	Lattice symmetry	Cell parameters			
			a (Å)	b (Å)	c (Å)	V (Å^3)
900	0.0	Rhombohedral	5.515	–	13.328	351.2
	0.2	Orthorhombhic	5.446	5.517	7.759	233.1
	0.4	Orthorhombhic	5.439	5.523	7.767	233.3
	1.0	Orthorhombhic	5.525	5.549	7.825	240.0
1100	0.0	Rhombohedral	5.529	–	13.373	354.1
	0.2		5.529	–	13.372	354.0
	0.4		5.528	–	13.342	353.2

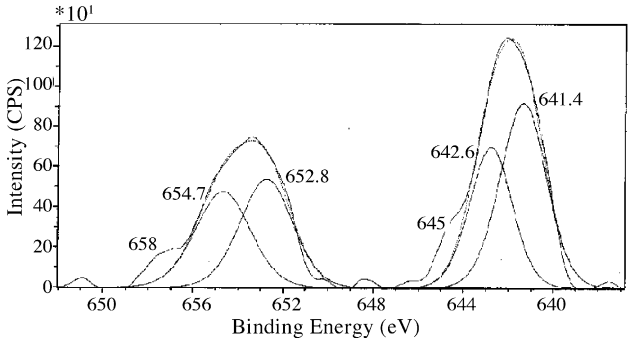

Fig. 2. Mn 2p XPS spectrum of $La_{0.8}Sr_{0.2}Mn_{0.8}Fe_{0.2}O_{3-\delta}$ (LSMF2) catalyst.

Table 3
Representative XPS binding energy values of different elements in $La_{0.8}Sr_{0.2}Mn_{0.8}Fe_{0.2}O_{3-\delta}$ sample at the external surface and after 20 min sputtering with Ar^+ ions of 3 KeV energy

	BE of XPS signal (eV)			
	La $3d_{5/2}$	Sr $3d_{5/2}$	Mn $2p_{3/2}$	Fe $2p_{3/2}$
No sputtering	834.5, 838.0	132.2	641.4, 642.6	710.1, 712.2
After sputtering	833.6, 837.6	132.5	640.8, 642.0	709.5, 711.2
Oxidation state	+3	+2	+4, +3.5	+2, +3

Table 3 gives the representative BE value of constituent elements of substituted LSM sample, without and after 20 min argon ion sputtering. Corresponding atom concentrations of these elements are included in Table 4. The XPS lines mentioned above indicate the presence of both iron and manganese in two distinct oxidation states. The lower BE line at 641.4 eV, shifting to a lower value of 640.9 ± 0.1 eV after sputtering, may be attributed to the presence of manganese in +4 oxidation state at surface and in +3 state in the bulk [24]. The 642.6 eV XPS line of 'as mounted' LSM oxides has been reported and discussed by various research groups and has been attributed to +3.5 oxidation state of Mn ions on the basis of various considerations such as the splitting of XPS s-lines [23]. The BE of this line decreases only marginally after sputtering (Table 3). The Fe 2p XPS emission lines from $La_{0.8}Sr_{0.2}Mn_{0.6}Fe_{0.4}O_{3-\delta}$ sample, appearing at BE values of around 709.5 and 711.2 eV (Fig. 3b), showed an almost identical separation of ~2.6 eV in their spin-orbital splitting doublets and may be attributed to the presence of bulk iron ions in the oxidation states of +2 and + 3, respectively [24]. On sputtering, the concentration of Fe^{2+} sites decreases considerably while that of the Fe^{3+} undergoes an increase. It is likely that the Fe^{2+} species, detected only at the surface could arise from $Fe^{3+} \rightarrow Fe^{2+}$ conversion under vacuum. Furthermore, the sputtering-dependent atom concentration data in Table 4 reveal that the iron segregation at the sample surface occurred only to a marginal extent.

3.3. Mössbauer spectroscopy

Room temperature Mössbauer spectra of LSMF samples are shown in curves a–c of Fig. 4 for there typical iron substitutions, i.e. for x values of 0.2, 0.4 and 0.6, respectively. A comparative spectrum for pure LSF phase is shown in curve d of this figure. The corresponding values of isomer shift are given in Table 5.

Mössbauer spectra reveal that Fe is present in trivalent state in all the substituted samples but its coordinative environment depended upon Fe content. Thus, the Mössbauer spectrum of $La_{0.8}Sr_{0.2}Mn_{0.8}Fe_{0.2}O_{3-\delta}$ (LSMF2) could be fitted into one symmetric doublet with a large quadrupole splitting (Q.S.) of ~0.48 mm s^{-1} and IS shift of ~0.33 mm s^{-1} (Fig. 4a). This paramagnetic doublet is attributed to the presence of Fe^{3+} ions in an octahedral oxygen lattice [25]. With increasing iron content in samples LSMF4 and LSMF6, a gradual transition from paramagnetic to magnetic (ferro- or antiferro-) can be noted. This is

Table 4
Relative atom concentration of different elements $La_{0.8}Sr_{0.2}Mn_{1-x}Fe_xO_{3-\delta}$ samples as a function of x value

Without sputtering							After sputtering					
x	La	Sr	Mn	Fe	O	Fe/La + Mn	La	Sr	Mn	Fe	O	Fe/La + Mn
0	20.2	3.3	3.6	–	72.8	–	21.5	3.4	5.7	–	69.3	–
0.2	17.0	3.4	3.2	2.5	–	0.15	24.8	4.1	5.6	2.9	62.5	0.12
0.4	16.1	3.4	4.0	3.2	73.1	0.16	23.0	4.9	5.3	4.3	62.3	0.18
0.6	16.5	3.0	3.8	5.5	71.2	0.27	23.1	4.6	5.9	5.3	61.0	0.23

Table 5
Mössbauer parameters of LSMF catalyst

Catalyst	Nature	H_{int} (kOe)	IS (±0.02) (mm s^{-1})	Q.S. (mm s^{-1})	Relative intensity (%)
LSMF2	Paramagnetic	–	(a) 0.33	0.48	100
LSMF6	Paramagnetic	–	(a) 0.302	0.438	16.31
	Magnetic (I)	450.6	(b) 0.404	0.043	40.62
	Magnetic (II)	383.0	(c) 0.308	0.062	43.05
LSF	Paramagnetic	–	(a) 0.183	0.027	18.88
	Magnetic (I)	511.4	(b) 0.409	0.024	27.93
	Magnetic (II)	441.6	(c) 0.369	0.054	53.18

reflected clearly in the presence of two hyperfine-split sextets in addition to the above-mentioned doublet in curves b and c of Fig. 4. The isomer shift for these sextets varies between 0.3 and 0.4 and the sextets match with that observed for pure LSF (curve d) phase, in terms of the isomer shift and the quadrupole splitting values, as shown in Table 5. These two sextets, appearing at magnetic fields of ∼450.6 and 383 kG may be ascribed to Fe^{3+} cations located at distorted octahedral sites, thus, suggesting the existence of domains/regions with varying local fields. This distortion in symmetry may arise due to anisotropic deformation of the environment of the Fe^{3+} ions due to oxygen vacancies generated by substitution at Mn sites. These results, thus, reveal the presence of iron in at least three distinct environments, the relative concentration of which may depend upon Fe-content. The Mössbauer spectroscopy results also show that the hyperfine field (H_{int}) increased progressively, as one goes to LSF from LSMF6, indicating that Fe is more magnetically ordered in LSF. This is, further, supported by the lower Q.S. values for LSF samples as compared to LSMF6.

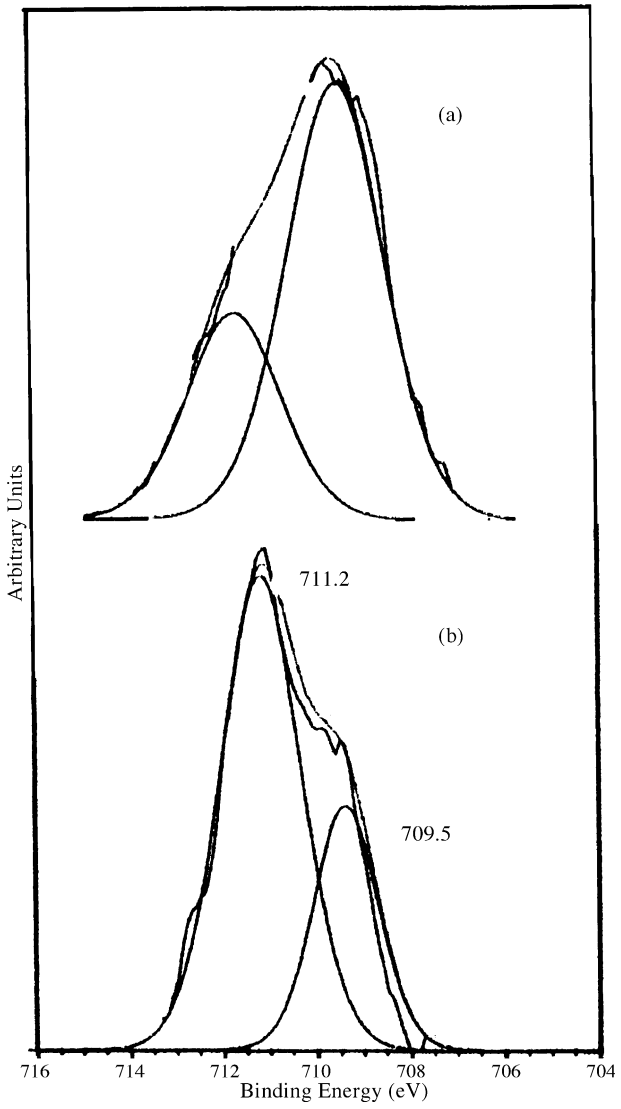

Fig. 3. Fe 2p XPS spectra of $La_{0.8}Sr_{0.2}Mn_{0.8}Fe_{0.2}O_{3-\delta}$ (LSMF2): (a) without sputtering and (b) after 10 min sputtering.

3.4. TPR

The reduction profiles (TPR) of LSM along with its iron-substituted homologues are presented in Fig. 5a–f. The reduction profile of LSM (Fig. 5a) shows at least two clear reduction stages, first at 350–600 °C and the second stage in the wide temperature interval of 700–980 °C. We may mention that Mn is the only reducible species in the case of LSM sample. This profile clearly indicates the existence of two distinct manganese sites, corresponding to XPS bands mentioned above (Fig. 2). Such multiple reduction stages have been reported earlier by Buciuman et al. [26] in case of TPR study on $LaMnO_{3.16}$ samples,

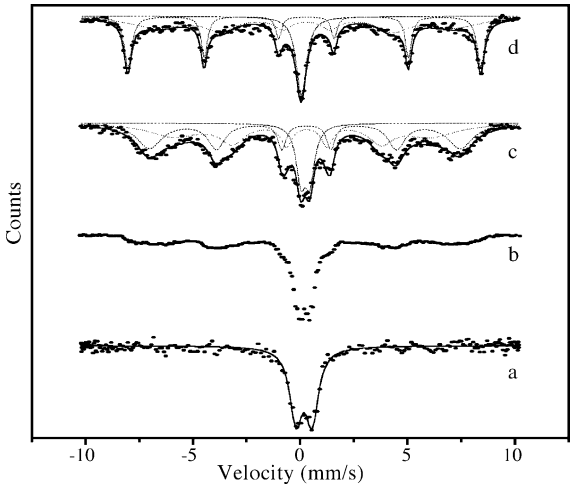

Fig. 4. Mössbauer spectra of LSMF catalysts of various compositions: (a) LSMF2, (b) LSMF4, (c) LSMF6 and (d) LSF.

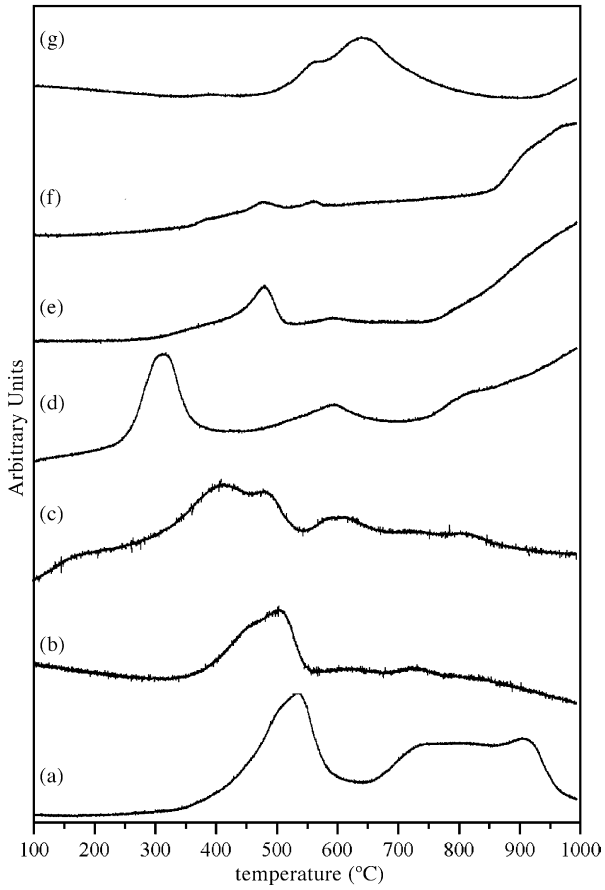

Fig. 5. TPR profiles of different LSMF samples synthesized by solution route. Curves (a) LSM, (b) LSMF2, (c) LSMF4, (d) LSMF6, (e) LSMF8 and (f) LSF. Curve (g) shows TPR profile of a LSMF2 sample synthesized by solid-state route.

having substitution at A site with Sr, Ba, K and Cs. It has been demonstrated by these authors that Mn is present in +4 as well as in +3 states and the Mn^{4+} state reduces at a lower temperature as compared to Mn^{3+}. This has been interpreted in terms of lowering of the oxidative nonstiochiometry on substitution of La^{3+} by cations at lower oxidation stage, while keeping the tetravalent manganese practically unchanged. Since our sample shows rhombohedral symmetry, the reduction of strontium substituted lanthanum manganites is likely to follow the scheme:

$$La_{0.8}{}^{3+}Sr_{0.2}{}^{2+}Mn_x{}^{4+}Mn_{1-x}{}^{3+}O_{3.16} \xrightarrow{350\,^\circ C} La_{0.8}{}^{3+}Sr_{0.2}{}^{2+}Mn^{3+}O_{2.9}$$

$$La_{0.8}{}^{3+}Sr_{0.2}{}^{2+}Mn^{3+}O_{2.9} \xrightarrow{700\,^\circ C} 0.4La_2O_3 + 0.4MnO + 0.2SrMn_3O_{6-\delta}$$

The reaction schemes mentioned above were validated by the XRD pattern of the TPR residue of LSM that showed the presence of La_2O_3, MnO and $SrMn_3O_{6-\delta}$. We, therefore, conclude that the low temperature reduction in Fig. 5 arises due to $Mn^{4+} \rightarrow Mn^{3+}$ conversion and at a high temperature, i.e. above 600 °C, it is due to Mn^{3+} to Mn^{2+}.

In case of sample LSMF2 where Fe substitutes a part of Mn, the overlapping TPR bands in 400–600 °C region shift to lower temperature while the intensity of the high temperature bands (700–900 °C) decreased considerably (Fig. 5b). This temperature shift becomes more prominent (∼200 °C) with further increase in x-value to 0.6 (Fig. 5d). The low intensity TPR bands in Fig. 5e and f indicates that the reduction of Fe^{3+} cations may occur only at temperatures above 800 °C. These results suggest the generation of certain micro-structural defects in the vicinity of Mn sites as a result of iron substitution, thus, promoting the diffusion through the bulk and eventually facilitating the reduction. This inference is supported by the XRD results showing a clear change in symmetry from rhombohedral to orthorhombic, which is known to be an oxygen deficient structure. The shift in T_{max} from 300 °C in case of LSMF6 sample to a higher temperature of ∼500 °C for LSMF8 may be attributed to increase in symmetric ordering of Fe as we go from LSMF6 to LSF sample as indicated by Mössbauer spectroscopy results.

In addition to the role of Fe substitution as described above, the reduction profile of a sample depended upon the particle morphology as well. Thus, a shift to higher temperature by ∼150 °C was noticed in the TPR profile of a representative $La_{0.8}Sr_{0.2}Mn_{0.8}Fe_{0.2}O_{3-\delta}$ sample, synthesized by solid-state route and having larger particle size (Table 1). To enable a comparison, these results are presented in curve g of Fig. 5. The increase in reduction temperature as seen in Fig. 5g, thus, indicates an important role of sample crystallite size in reduction behavior.

3.5. Catalytic activity

Fig. 6 presents the catalytic activity of LSMF samples, synthesized at a calcination temperature of 900 °C, for CO oxidation reaction. As seen in curves b–d of this figure, the iron containing samples exhibited better catalytic activity as compared to unsubstituted LSM (curve a) or the sample of other extreme composition, i.e. LSF (curve e). For instance, Fe-containing samples exhibited ca. 90–100% conversion of CO to CO_2 at 400 °C while only 45% conversion was observed using LSM at this reaction temperature. Not only an increase was observed in the conversion, the reaction onset temperature was also found to decrease as a result of iron substitution (Fig. 6b–d). The highest CO conversion of ∼100% at 350 °C, was exhibited by $La_{0.8}Sr_{0.2}Mn_{0.4}Fe_{0.6}O_{3-\delta}$ (LSMF6) catalyst and this is in line with the considerable lowering of reduction temperature in its TPR profile (Fig. 5d).

As in the case of TPR results described above, the catalytic activity was also influenced considerably by the physical characteristics of a particular Fe-substituted sample. Curves a and b in Fig. 7 exhibit the catalytic activity of a representative $La_{0.8}Sr_{0.2}Mn_{0.8}Fe_{0.2}O_{3-\delta}$ (LSMF2) sample synthesized by using two different routes. For instance, the sample synthesized by solid-state method and having larger size particles gave rise to much lower $CO \rightarrow CO_2$ conversion (curve b), as compared to corresponding sample synthesized through solution route (curve a). This indicates again the importance of crystallite size in the catalytic properties of metal oxide systems.

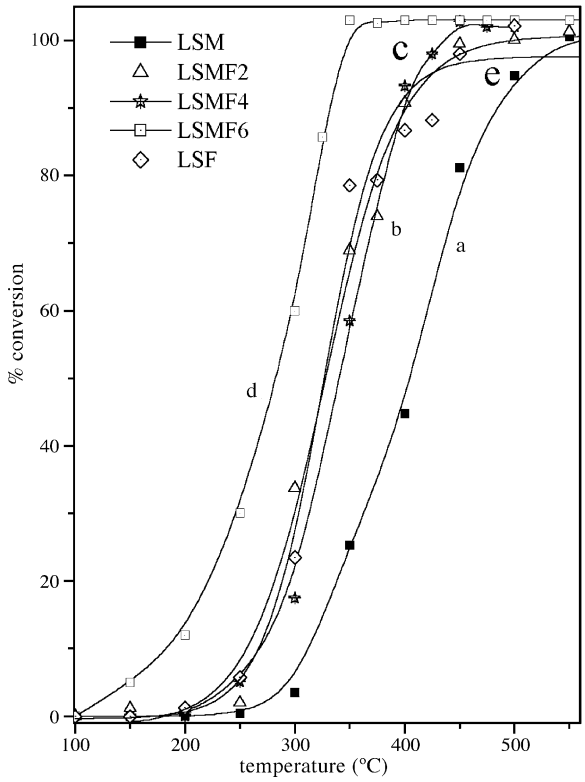

Fig. 6. Catalytic activity of $La_{0.8}Sr_{0.2}Mn_{1-x}Fe_xO_{3-\delta}$ catalysts for CO oxidation reaction. Curves (a) LSM, (b) LSMF2, (c) LSMF4, (d) LSMF6 and (e) LSF.

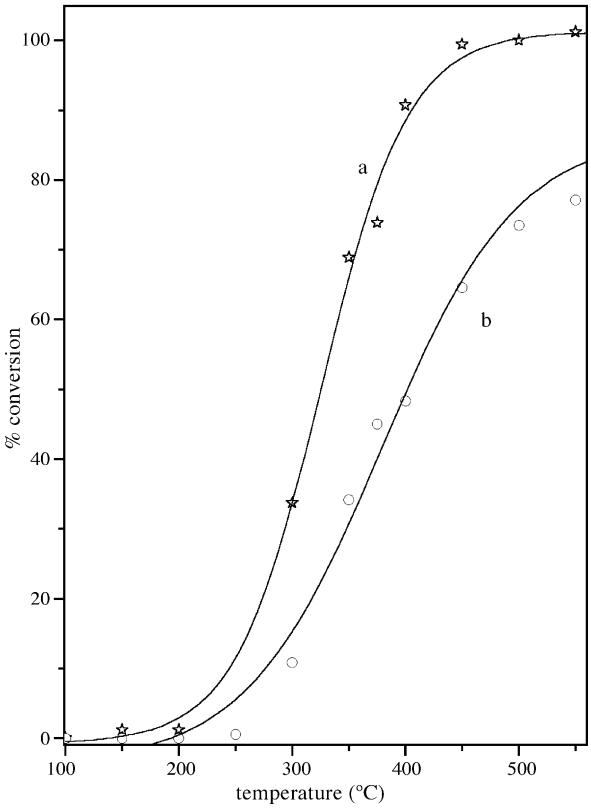

Fig. 7. Catalytic activity of $La_{0.8}Sr_{0.2}Mn_{0.8}Fe_{0.2}O_{3-\delta}$ (LSMF2) sample synthesized by different routes: (a) nitrate route and (b) solid-state route.

4. Discussion

The influence of synthesis route and that of the substitutions at cation sites on the catalytic and electro-catalytic properties of mixed metal oxides has been highlighted in several previous publications; even though discrepant views have been expressed in regards to the nature of the physico–chemical properties that are responsible to the catalytic behavior of these materials [27,28]. For instance, the difference in CO oxidation activity of $La_{1-x}Sr_xMnO_3$ samples synthesized through six different routes has been ascribed to certain micro-structural surface properties rather than the physical characteristics such as the particle size and surface area [27]. Effect of partial substitution on catalytic activity of $La_{0.7}Sr_{0.3}Co_{1-x}Fe_xO_3$ perovskites has similarly been attributed to the degree of certain structural disorders (grain boundary, etc.) and at the same time the role of chemical composition and the surface enrichment has been ruled out [4]. On the other hand, the enhancement in activity of La–Cu–Fe–O mixed oxides for CO + NO reaction has been correlated to the substitution-induced surface concentration of metallic copper in a recent study by Peter et al. [9]. The catalytic properties of mixed metal oxide systems have also been attributed to other properties such as crystal structure, non-stoichiometry resulting from substitutions at A- or B-sites, oxygen ion mobility, oxygen storage capacity and redox properties, etc. [18–20,29,30]. At the same time, the influence of powder morphology on the catalytic activity of mixed metal oxides has been emphasized in some of the recent studies. For instance, Taguchi et al. [31] have demonstrated that the low temperature synthesis by citrate route led to decreased crystallite size of La–Ca–Fe–O perovskites and such samples exhibited a higher catalytic activity. Ma et al. [32] have similarly reported that the spinel-type $Mg_xFe_{3-x}O_4$ catalysts with greater non-stoichiometry and smaller particle size exhibited better activity for styrene oxidation reaction.

The results obtained in the present study clearly reveal a definite relationship between the catalytic activity of mixed metal oxides and certain morphological and structural changes caused either by the substitutions or by adopting a low-temperature synthesis route. The following are the highlights of our results:

1. The substitution of Fe in place of Mn caused a rearrangement in the symmetry of the parent LSM perovskite. Thus, the substituted samples exhibited an orthorhombic symmetry instead of the rhombohedral symmetry of the unsubstituted counterpart.
2. Commensurate to the change of symmetry, a considerable decrease was observed in the cell parameters and the cell volume of Fe-substituted samples (Table 2). Also a significant decrease was observed in the crystallite size of LSMF samples (Table 1), synthesized through solution route and calcined at relatively lower temperature.
3. XPS results show no significant surface segregation of constituent metal. At the same time, Fe-substitution resulted in the formation of high-valence B-cation, i.e. Mn^{4+}. Such

high-valent B-cation in the perovskite structure ABO_3 are known to influence various bulk and surface properties. For instance, B^{4+} cations, i.e. Fe^{4+} and Mn^{4+}, are reported to play an important role in the catalytic, electric and ionic transport properties of LSM oxides due to the presence of B^{3+}–O–B^{4+} couples and associated oxygen in vacancies in the lattice [33]. A recent Mössbauer spectroscopy study of Abdelmoula et al. [25] has indeed demonstrated a significant increase in concentration of oxygen ion vacancies as a result of Fe substitution in LSM materials that facilitates the anionic diffusion.

4. TPR results confirm a direct influence of decreased particle size and the substitution-induced non-stoichiometry on the lowering of reduction temperature of LSM samples.
5. The samples synthesized through low-temperature routes and comprising of smaller size particles exhibited higher catalytic activity for CO oxidation reaction.

On the basis of above observations, we may infer that the reduction behavior and the catalytic activity of LSMF samples are influenced by a combination of factors, such as the symmetry and the valence state of B-site cations, substitution-induced non-stoichiometry leading to improved transport of bulk oxygen ions and the crystallite size of the samples that depends upon the adopted synthesis procedure. Thus, the decrease in CO conversion and increase in reduction temperature from LSMF6 to LSF sample may be attributed to increase in symmetric ordering of Fe in case of LSF sample, as indicated by Mössbauer results (Fig. 4). As is well documented, the particle size is an important parameter influencing the catalytic properties. The smaller size crystallites of nanometer scale not only exhibit higher dispersity and greater specific surface area; their surface properties may also be different from their bulk analogues. Our study clearly provides evidence that the powder morphology of a mixed oxide samples, i.e. crystallite size, surface area and surface micro-structure, may depend considerably on the nature of the constituent cation and the procedure adopted for the synthesis of a particular sample.

5. Conclusion

The substitution of Fe is found to have considerable influence upon the catalytic activity of LSM for CO oxidation reaction. Based on the above results, we may conclude that the lowering of T_{max} in Fig. 5 and the enhancement of catalytic activity in case of LSMF samples (Figs. 6 and 7) is governed by a combination of factors, such as: (i) a smaller crystallite size giving rise to larger surface area and hence in enhanced number of reaction sites, (ii) greater non-stoichiometry caused by substitution of an aliovalent cation at B site facilitating the lattice oxygen diffusion via anionic vacancies generated in the process, and (iii) a change in the symmetry around a constituent cation.

References

[1] H. Arai, M. Machida, Catal. Today 10 (1991) 81.
[2] M.F. Zwinkels, S.G. Jaras, P.G. Menon, Catal. Rev. Sci. Eng. 35 (3) (1993) 319.
[3] L. Forni, C. Oliva, F.P. Vatti, M.A. Kandala, A.M. Ezerets, A.V. Vishniakov, Appl. Catal. B: Environ. 7 (1996) 269.
[4] I.A. Isupova, V.A. Sadykov, S.V. Tsybulya, G.N. Kryukova, V.P. Ivanov, A.N. Petrov, O.F. Kononchuk, React. Kinet. Catal. Lett. 62 (1997) 129.
[5] L. Forni, C. Oliva, T. Brazetti, E. Selli, A.M. Ezerets, A.V. Vishniakov, Appl. Catal. B: Environ. 13 (1997) 35.
[6] L. Marchetti, L. Forni, Appl. Catal. B: Environ. 15 (1998) 179.
[7] L. Lisi, G. Bagnasco, P. Ciambelli, S.D. Rossi, P. Porta, G. Russo, M. Turco, J. Solid State Chem. 146 (1999) 176.
[8] H.X. Dai, C.F. Ng, C.T. Au, J. Catal. 189 (2000) 52.
[9] S.D. Peter, E. Garbowski, V. Perrichon, B. Pommier, M. Primet, Appl. Catal. A: Gen. 205 (2001) 147.
[10] Y. Zhang-Steenwinkel, J. Beckers, A. Bliek, Appl. Catal. A: Gen. 235 (2002) 79.
[11] S. Varma, B.N. Wani, N.M. Gupta, Appl. Catal. A: Gen. 205 (2001) 295.
[12] M.R. Pai, B.N. Wani, N.M. Gupta, J. Mater. Sci. Lett. 21 (2002) 1187.
[13] S. Varma, B.N. Wani, N.M. Gupta, Mater. Res. Bull. 37 (2002) 2117.
[14] S. Varma, B.N. Wani, N.M. Gupta, Appl. Catal. A. 241 (2003) 341.
[15] S. Varma, B.N. Wani, A. Sathyamoorthy, N.M. Gupta, J. Phys. Chem. Solid 65 (2004) 1291.
[16] M.R. Pai, B.N. Wani, N.M. Gupta, J. Mol. Catal. A 223 (2004) 275.
[17] M.R. Pai, B.N. Wani, N.M. Gupta, Thermochim. Acta 425 (2005) 109.
[18] R.J.H. Voorhoeve, Advanced Materials in Catalysis, Academic Press, New York, 1997, p. 129.
[19] L.G. Tejuca, J.L.G. Fierro, J.M.D. Tascon, Adv. Catal. 36 (1989) 237.
[20] H. Tanaka, M. Misono, Curr. Opin. Sol. Stat. Mater. Sci. 5 (2001) 381.
[21] G. Caboche, L. Dufour, F. Morin, Solid State Ionics 144 (2001) 211.
[22] Q.H. Wu, M. Liu, W. Jaegermann, Mater. Lett. 59 (2005) 1480.
[23] W. Wang, J.B. Zhang, G.D. Lin, Z.T. Xiong, Appl. Catal. B: Environ. 24 (2000) 219.
[24] C.D. Wagner, W.M. Riggs, L.E. Davis, J.F. Moulder, G.E. Muilenberg, Handbook of X-ray Photoelectron Spectroscopy, Perkin-Elmer Corporation, USA, 1979.
[25] M. Abdelmoula, M. Petitjean, G. Caboche, J.-M. Genin, L.C. Dufour, Hyperfine Inter. 156/157 (2004) 299.
[26] F.C. Buciuman, F. Patcas, J. Zsako, J. Thermal. Anal. Calorim. 61 (2002) 819.
[27] R.J. Bell, G.J. Millar, J. Drennan, Solid State Ionics 131 (2000) 211.
[28] J. Sfeir, S. Vaucher, P. Hotappels, U. Vogt, H.-J. Schindler, J. Van herle, E. Suvorova, P. Buffat, D. Perret, N. Xanthopoulos, O. Bucheli, J. Europ. Ceram. Soc. 25 (2005) 1991.
[29] H. He, H.X. Dai, K.W. Wong, C.T. Au, Appl. Catal. A: Gen. 251 (2003) 61.
[30] A. Delmastro, D. Mazza, S. Ronchetti, M. Vallino, R. Spinicci, P. Brovetto, M. Salis, Mater. Sci. Eng. B 79 (2001) 140.
[31] H. Taguchi, Y. Masunaga, K. Hirota, O. Yamaguchi, Mater. Res. Bull. 40 (2005) 773.
[32] N. Ma, Y. Yue, W. Hua, Z. Gao, Appl. Catal. A: Gen. 251 (2003) 39.
[33] M. Petitzean, G. Caboche, E. Siebert, L. Dessemond, L.-C. Dufour, J. Europ. Ceram. Soc. 25 (2005) 2651.